Raman scattering from one- and two-magnons in magnetoelectric $LiNiPO_4$

D. Rigitano,[1] D. Vaknin,[2] G. E. Barberis,[1] and E. Granado[1]

[1] *"Gleb Wataghin" Institute of Physics, University of Campinas - UNICAMP, Campinas, São Paulo 13083-859, Brazil*
[2] *Ames Laboratory, US-DOE, and Department of Physics and Astronomy, Iowa State University, Ames, Iowa 50011, USA*

Polarized Raman scattering in magnetoelectric $LiNiPO_4$ shows a sharp resonant peak at 37 cm^{-1} in the magnetically ordered phase, originating from a one-magnon excitation of Ni^{2+} $S = 1$ localized moments at the zone center. Also, a broad component with maximum intensity at $\sim$ 65 cm^{-1} is observed and successfully modeled in terms of light scattering from two-magnon excitations within the framework of the Fleury-Loudon theory using five relevant exchange parameters, providing an independent experimental confirmation of their values previously obtained with inelastic neutron scattering data in this material. An additional excitation at 58 cm^{-1}, already reported in previous works, shows no detectable Zeeman splitting for magnetic fields up to 6 T along the crystallographic **a** and **c** directions, constraining its origin.

I. INTRODUCTION

The lithium orthophosphate of nickel is a member of the family of olivines with chemical formula $LiMPO_4$ (M= Ni, Co, Mn and Fe). These insulating compounds show orthorhombic crystal structure with *Pnma* space group at zero magnetic field [see Fig. 1(a)] and presents a sizable magnetoeletric (ME) effect below the magnetic ordering temperature [1–3]. These materials also attract large interest for their use as Li batteries [4].

In $LiNiPO_4$, the Ni^{2+} magnetic moments are nearly oriented along the **c** axis with a small canting towards the **a** axis in the magnetically ordered phase below T_N = 20.8 K [5]. Microscopic treatments including symmetric Heisenberg and antisymmetric Dzyaloshinsky-Moriya exchange interactions as well as quadratic spin anisotropy terms and Zeeman coupling with the external magnetic field are able to quantitatively capture the magnetoelectric coupling in this material [5, 7, 8]. Spin wave dispersion investigations of the $LiNiPO_4$ in the magnetically ordered phase were performed using inelastic neutron scattering (INS) measurements [9–11]. A simplified Heisenberg Hamiltonian including five nearest-neighbor coupling constants (see Fig. 1(b)) summed with two anisotropy terms was considered to represent the minimum spin model to capture the INS data, thus leading to seven free parameters. This relatively large number of fitting parameters calls for complementary techniques to confirm the magnetic constants. For instance, two-magnon Raman scattering data [12], modeled with the aid of the Fleury-Loudon (FL) theory [13], were shown to be decisive in choosing between two largely different sets of magnetic constants that could fit equally well the reported spin-wave dispersion obtained by INS data in $LiMnPO_4$ [12]. Also, spin resonances observed by infrared absorption spectroscopy as a function of magnetic field has been recently shown to provide yet another means of accessing the exchange constants of $LiNiPO_4$ [14].

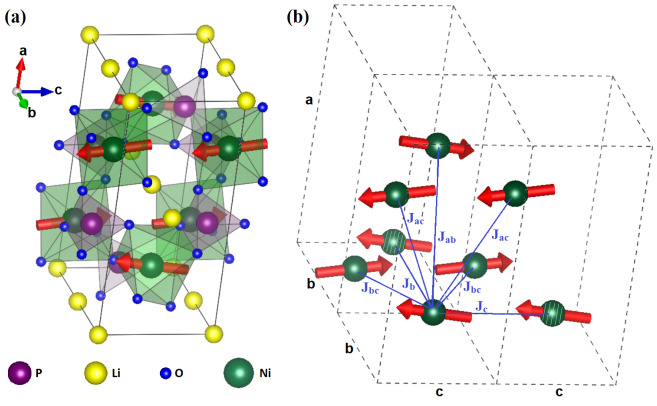

FIG. 1: (a) Orthorhombic unit cell of $LiNiPO_4$ (space group Pnma No. 62) with lattice parameters a = 10.02 Å, b = 5.83 Å, and c = 4.66 Å (Ref. [6]). The magnetic structure is composed by Ni^{2+} magnetic moments oriented along the **c** axis with a small canting along the **a** axis [5]. (b) Detailed view of the magnetic structure and definition of the most important magnetic exchange paths between Ni^{2+} moments, namely J_b, J_c, J_{ab}, J_{ac}, and J_{bc}.

Polarized Raman spectra of $LiNiPO_4$ single crystals have been previously studied by Fomin *et al.* [15] and Paraguassu *et al.* [16]. Raman-active phonon modes were observed and classified according to their symmetry, and additional excitations related to magnetic order have also been reported in the spectral range between $\sim$ 50 and 80 cm^{-1} [15]. Nonetheless, an unambiguous assignment and a quantitative analysis of the magnetic Raman signal are still missing. Also, Raman measurements under applied magnetic fields have not been carried out so far in this magnetoelectric material.

In this paper, we report a polarized Raman study of $LiNiPO_4$ with application of magnetic field along both the **a** and **c** axes. The magnetic Raman signal is observed below T_N and assigned to one-magnon and two-magnon excitations. Enlightened by the FL theory of light scattering by magnetic excitations, the two-magnon scattering is modeled, confirming the previously published INS exchange parameters [9, 10] within statistical uncertainty. The possible nature of an interesting additional

excitation at 58 cm^{-1} is discussed in detail.

II. EXPERIMENTAL DETAILS

The $LiNiPO_4$ single crystal employed in this work was grown by a flux technique as described elsewhere [15]. The chosen crystal was taken from the same batch as the one used for the previous INS study [9], and has a thin rectangular surface perpendicular to the **a** direction with sides coincident with the **b** and **c** directions. Raman scattering measurements were performed on a Jobin Yvon T64000 triple 1800 mm^{-1} grating spectrometer equipped with a liquid N_2-cooled multichannel CCD detector, using $\lambda = 514.5$ and 532 nm excitation lines obtained with a Spectra Physics Ar^+/Kr^+ gas and a Cobolt 08-DPL 532 nm diode laser, respectively, in a quasi-backscattering configuration. Laser linewidths are below 1 MHz for both lines. The crystal was mounted with a flat surface oriented in the *bc* plane nearly perpendicular to the incident beam direction, therefore the probed polarizations in our experiments are (Porto's notation) $X(YY)\bar{X}$, $X(ZZ)\bar{X}$, and $X(ZY)\bar{X}$; thus, for simplicity, only the incident and scattered polarizations [YY, ZY or ZZ] are indicated in the following. The sample was kept within a superconducting magnetocryostat with optical windows, and the temperature control was achieved by helium flow under low pressure. The magnetic field was applied along the **a** and **c** crystallographic directions. The sample was mounted in such a way that the **b** direction is orthogonal to the grooves of the diffraction gratings of the spectrometer, corresponding to optimal instrumental efficiency for the experiments with the scattered light polarization along this direction, with $\lambda = 532$ nm, whereas the **c** direction is orthogonal to such grooves for the experiments with $\lambda = 514.5$ nm. Consequently, the spectra under YY and ZZ polarizations were only taken with $\lambda = 532$ and 514.5 nm, respectively. These selected geometries for each wavelength also limited our choice of directions for the magnetic field with respect to the crystalline axes. The large focal distance of the focusing lens (300 mm) placed outside the magnet led to focal spots of ~ 200 μm diameter. Whereas preliminary tests showed no significant heating effect for laser power up to at least 40 mW, the power was kept below ~ 15 mW for the spectra shown in this manuscript. The relatively large focal spots ultimately set the lower limit of the spectral range available in this specific work (~ 25 cm^{-1}).

III. RESULTS AND ANALYSIS

Figures 2(a)-2(d) show the Raman spectra of $LiNiPO_4$ in the whole spectral region investigated in this work, i.e., $25 \lesssim \omega < 700$ cm^{-1}, at temperatures below and above T_N, for ZY polarization with $\lambda = 532$ nm (a), ZY polarization with $\lambda = 514.5$ nm (b), YY polarization with $\lambda = 532$ nm (c), and ZZ polarization with $\lambda = 514.5$ nm (d). Besides the main phonon A_g modes at 177, 308, 582 and 643 cm^{-1} and the B_{3g} modes at 122, 194, 262, 330, 443, and 593 cm^{-1}, additional low frequency signal ($\omega < 100$ cm^{-1}) is observed below T_N, which is of particular interest for this study. Figures 3(a)-3(d) show in more detail the observed Raman spectra of $LiNiPO_4$ in the low

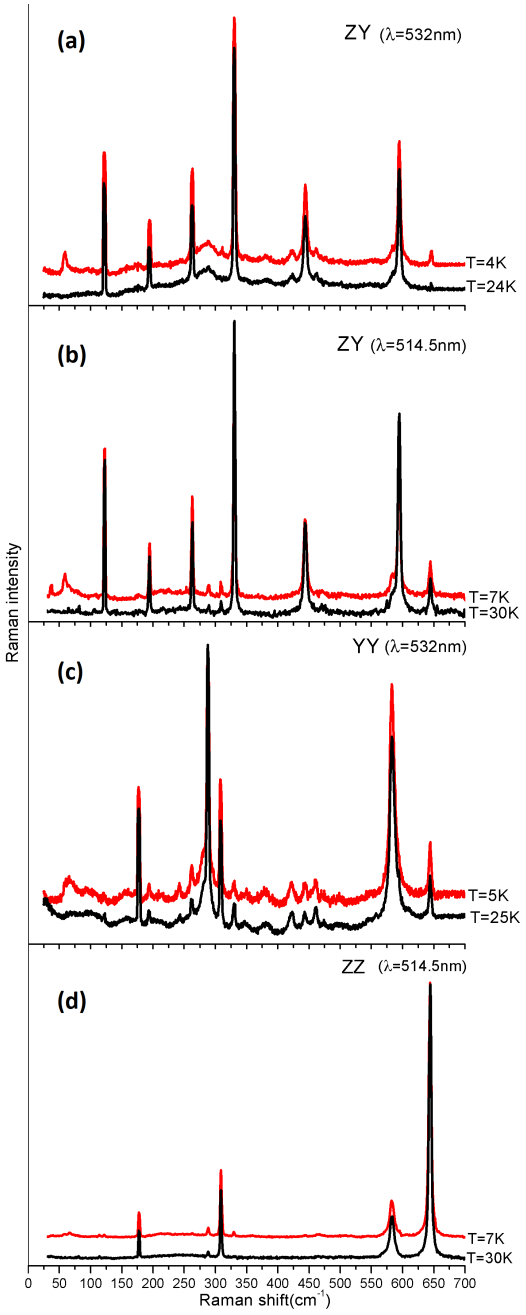

FIG. 2: Polarized Raman spectra below and above $T_N = 20.8$ K with ZY polarization, $\lambda = 532$ nm (a); ZY polarization, $\lambda = 514.5$ nm (b); YY polarization, $\lambda = 532$ nm (c); and ZZ polarization, $\lambda = 514.5$ nm (d).

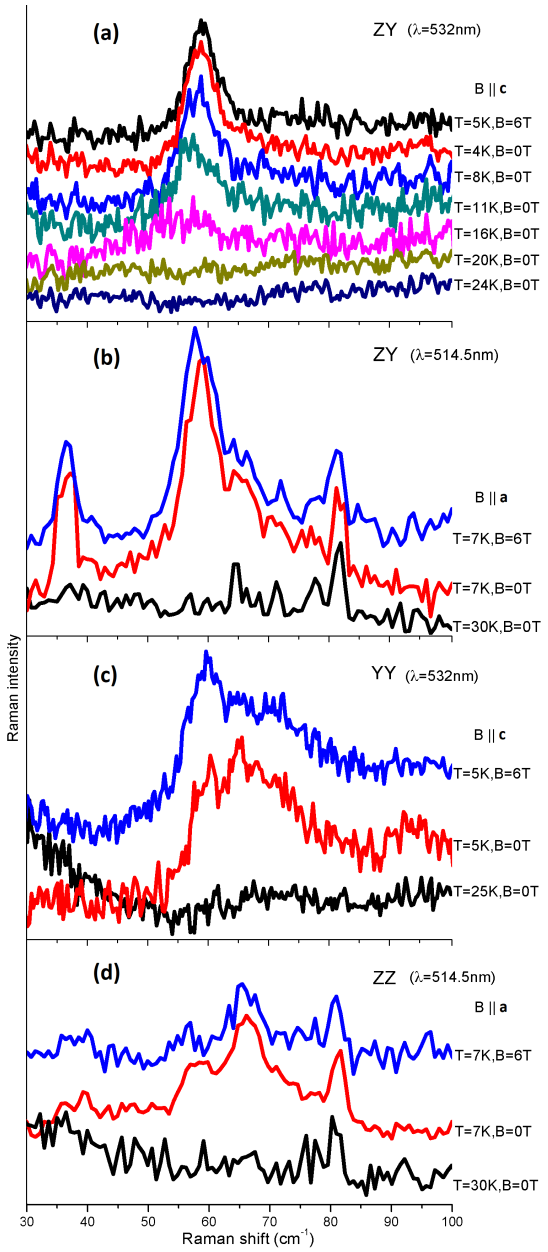

FIG. 3: Polarized low-frequency Raman spectra below and above $T_N = 20.8$ K with and without application of magnetic field. ZY polarization, $\lambda = 532$ nm, $\mathbf{B} \parallel \mathbf{c}$ (a); ZY polarization, $\lambda = 514.5$ nm, $\mathbf{B} \parallel \mathbf{a}$ (b); YY polarization, $\lambda = 532$ nm, $\mathbf{B} \parallel \mathbf{c}$ (c); and ZZ polarization, $\lambda = 514.5$ nm, $\mathbf{B} \parallel \mathbf{a}$ (d). The peak at 81 cm^{-1} in (b) and (d) is ascribed to a laser plasma line.

frequency region, either with or without a magnetic field of 6 T, in the same polarizations and wavelengths shown in Fig. 2(a)-2(d) and with (a) $\mathbf{B} \parallel \mathbf{c}$; (b) $\mathbf{B} \parallel \mathbf{a}$; (c) $\mathbf{B} \parallel \mathbf{c}$; and (d) $\mathbf{B} \parallel \mathbf{a}$. The spectral features observed below T_N are: (i) a sharp peak at 37 cm^{-1} in ZY polarization for $\lambda = 514.5$ nm, (ii) a broad component centered at ~ 65 cm^{-1}, and (iii) a peak at 58 cm^{-1}. These features are discussed in more detail below.

A. One-magnon scattering

First-order Raman scattering from magnetic excitations (one-magnon scattering) is allowed as long as linear momentum is conserved, meaning that zone-center magnons can be created by an inelastic light scattering process [17]. According to the scattering mechanism involving electric-dipole coupling of the radiation to the crystal, the process is resonant when the energy of the incident or scattered photon matches the energy of an electronic transition involving states with $\Delta l \pm 1$ (Ref. [13]).

For $LiNiPO_4$, the resonant ($\lambda = 514.5$ nm) sharp feature observed at 37 cm^{-1} in ZY polarization at low temperatures corresponds to an energy of 4.5 meV, matching the zone-center energy of a magnon branch in the spin-wave spectra of this material [9, 10]. It also matches the energy of magnetic-dipole active excitation observed by infrared absorption spectroscopy [14]. We therefore associate this feature in our data to one-magnon Raman scattering. Notice that this peak is not observed with $\lambda = 532$ nm (Fig. 3(a)) or with $\lambda = 632.8$ nm (ref. [15]), demonstrating its strong resonant character. Application of a magnetic field of 6 T along the **a**-direction does not influence this peak significantly (see Fig. 3). This is indeed consistent with one-magnon scattering considering that the moment direction in the magnetic structure is nearly along **c** (see Fig. 1), i.e., perpendicular to the magnetic field direction.

B. Two-magnon scattering

The broad Raman scattering component with a maximum intensity at $\sim$ 65 cm^{-1} [see Figs. 3(a-d)] falls within the expected energy range for two-magnon scattering. Application of magnetic fields up to 6 T along the **a** and **c** directions does not change the two-magnon profiles appreciably [see Figs. 3(a-d)], indicating that they correspond to $S = 0$ excitations.

Following Ref. [12], the FL theory of two magnon Raman scattering [13] is employed to simulate the polarized Raman profile for a given set of exchange constants. Then, a simulated annealing fitting procedure is employed to find the set of exchange and anisotropy constants that optimizes the comparison of calculated data with the experimental two-magnon Raman profile reported here, simultaneously with inelastic neutron scattering magnon dispersion curves reported in Ref. [9]. The details of this procedure are given in the Appendix. Figures 4(a)-4(c) show the comparison of the observed Raman profiles in ZZ (a), ZY (b) and YY (c) polarizations with the calculated profiles, yielding good agreements. The fitted exchange parameters, in meV, are $J_b = 0.69(2)$, $J_c = -0.087(9)$, $J_{ab} = 0.37(9)$, $J_{ac} = -0.07(1)$, and $J_{bc} = 1.00(2)$ [see Fig. 1(b)], and

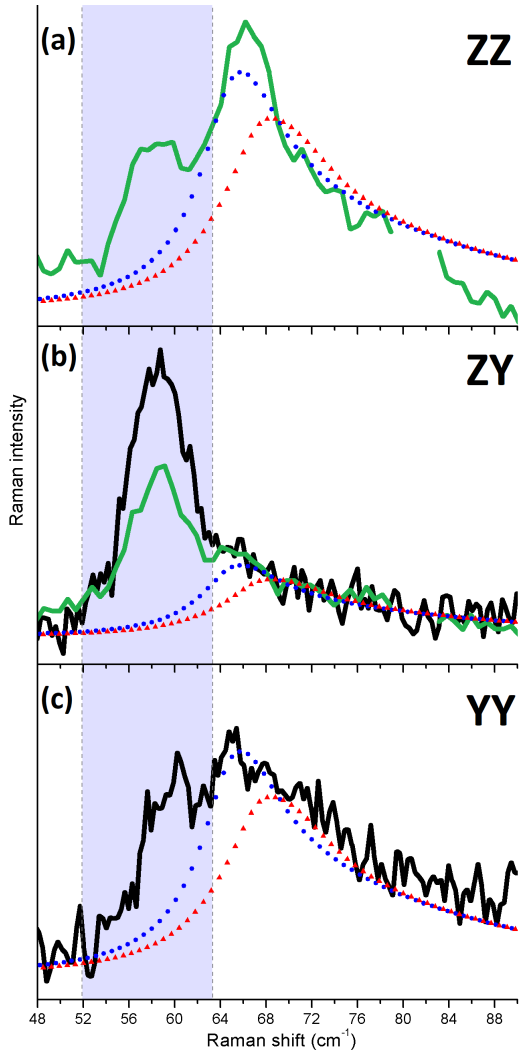

FIG. 4: Experimental Raman spectra in ZZ polarization with $\lambda = 514.5$ nm (a), ZY polarization with $\lambda = 514.5$ nm (b) and YY polarization with $\lambda = 532$ nm (c) in a selected frequency range covering the two-magnon excitations, at zero magnetic field and low temperatures (solid lines), in comparison to calculated two-magnon profiles using an optimized set of exchange constants (blue dotted line, see text) and the set of constants given in Ref. [9] (red dotted line). The marked spectral region between 52 and 63.5 cm^{-1} was excluded from the two-magnon fitting model due to the additional excitation observed at 58 cm^{-1}, not captured by our model.

the single-ion anisotropy terms are $D_x = 0.33(5)$ and $D_y = 1.80(4)$ meV. These values are fairly close to those reported by Jensen *et al.* [9] (a) and Li *et al.* [10] using the same simplified Hamiltonian, although the fitting of the Raman intensities is considerably better for the refined parameters given above [see Figs. 4(a)-4(c)]. We should mention that the simulated two-magnon profiles using the exchange parameters of Refs. [9] and [10] are very similar to each other, therefore only the former are provided in Figs. 4(a)-4(c).

C. Excitation at 58 cm^{-1}

In addition to the contributions reported above, a relatively strong signal is observed at 58 cm^{-1} below T_N, also reported in Ref. [15]. Amongst the probed symmetries, this signal has maximum intensity for ZY polarization, similarly to the one-magnon peak at 37 cm^{-1}. Some light on the identification of this peak is brought by a recent infrared spectroscopy study, in which this excitation was also observed below T_N and was found to be only electric-dipole-active, being ascribed to an electromagnon (ν_5 mode in Ref. [14]). A difficulty with such assignment is the fact that electromagnons are mixed electric/magnetic excitations that are linked to multiferroic states and in addition are normally observed for cicloidal magnetic structures, whereas $LiNiPO_4$ shows a commensurate canted magnetic structure and has not been reported to present a spontaneous ferroelectric polarization below T_N. On the other hand, the existence of a non-zero spontaneous magnetization below T_N and a detailed specific heat investigation of the first-order transition at $T_N = 20.8$ K led to a suggestion that the state below T_N is indeed a multiferroic state [18, 19].

The possibility of this excitation being associated with a soft phonon excitation that becomes zone-center by a magnetically-driven structural phase transition below T_N is also considered. Although such structural transition has not been reported by diffraction experiments so far, a minor lattice distortion cannot be ruled out, especially considering that the canted magnetic structure of $LiNiPO_4$ breaks the inversion symmetry of the orthorhombic *Pnma* structure [5]. In this scenario, considering the mutual exclusion principle of the Raman and infrared selection rules for centrosymmetric structures, the simultaneous Raman and infrared activity of the 58 cm^{-1} mode would be a direct consequence of such loss of inversion symmetry.

One may also speculate that the 58 cm^{-1} excitation may be part of the two-magnon scattering profile. Indeed, this energy is close to the two-magnon contribution identified above and in Fig. 4. On the other hand, the polarization-dependence of this component is markedly different from the two-magnon contribution centered at 65 cm^{-1} (see Fig. 3), whereas our simulations indicate that the two-magnon lineshapes and positions should be polarization-independent (see Appendix). Although the 58 cm^{-1} excitation is not captured by our model, we cannot exclude the possibility that a more complex magnetic Hamiltonian might lead to an additional peak in the two-magnon spectra.

Although we are not in position to choose amongst the above scenarios with the data presently at hands, the absence of a significant magnetic-field dependence of the position, lineshape or width of this peak for magnetic fields along both the **a** and **c** directions [see Figs. 3(a)

and 3(b)] severely constrains the possible explanations. For instance, a Zeeman splitting of the order 10 cm^{-1} for conventional one-magnon degenerate excitations would be expected with $\Delta S_z = \pm 1$ for $B = 6$ T along the moment direction in a two-sublattice spin model [13], which should be readily observable in our data [Fig. 3(a)]. Alternatively, in a non-collinear four-sublattice spin model, ~ 5 cm^{-1} shifts of different signs would be expected for each of the non-degenerate magnons, which is much more than our experimental resolution (~ 2 cm^{-1}). Therefore, a conventional one-magnon can be ruled out as the possible origin of the 58 cm^{-1} peak, and further investigations are needed to clarify the detailed nature of this excitation.

IV. DISCUSSION

Our experimental results show one- and two-magnon Raman scattering signals that constrains the magnetic exchange and anisotropy constants. In particular, our analysis of the two-magnon Raman spectrum confirms, considering the statistical uncertainties, the same magnetic constants previously obtained by INS studies [9, 10]. It is interesting to note that the two strongest exchange constants in $LiNiPO_4$ are J_b and J_{bc} [see section III.B and Fig. 1(b)], being both positive thereby favoring antiferromagnetic alignments along these directions. On the other hand, the magnetic structure of this material features a nearly antiferromagnetic alignment of the moments connected by J_{bc} and ferromagnetic alignment of those connected by J_b, implying a magnetic frustration due to competing interactions. This occurs because the strongest J_{bc} antiferromagnetic interaction geometrically constrains the alignment along **b** to be ferromagnetic despite the opposition of J_b.

V. CONCLUSIONS

In summary, polarized Raman scattering measurements on $LiNiPO_4$ show a sharp resonant one-magnon Raman peak at 37 cm^{-1} and a broad two-magnon signal centered at 65 cm^{-1}. An interesting additional peak at 58 cm^{-1} is also observed in the magnetically ordered phase. The two-magnon signal is shown to be consistent with the set of exchange and anisotropy parameters reported earlier based on INS data alone (Refs. [9] and [10]). Considering the large number of free parameters in the magnetic Hamiltonian of this system, our results provide a necessary and independent confirmation of the exchange parameters of this material, consolidating the current description of the magnetism in this system. This methodology may be extended to other complex magnetic systems. Finally, the detailed nature of the 58 cm^{-1} excitation still remains to be determined, although the insignificant field-dependence of this peak severely constrains the possible explanations.

Appendix A: Two-magnon Raman scattering calculations

Following Ref. [12], the FL theory of two magnon Raman scattering for $S = 0$ excitations [13] is employed to simulate the polarized Raman profile under a given set of exchange constants. In the following treatment, the small canting of the antiferromagnetic structure of $LiNiPO_4$ along **a** [see Fig. 1(a)] and the related antisymmetric terms in the magnetic Hamiltonian are ignored. In a collinear Heisenberg antiferromagnetic system with localized magnetic moments, the interaction between light and two-magnon excitations with $S = 0$ is given by the so-called Fleury-Loudon (FL) operator [13, 20, 21]:

$$\mathcal{O}_{\rm FL}^{(\mathbf{in})(\mathbf{out})} = \sum_{\langle \rm i,j \rangle} \rm J_{ij} (\hat{e}^{\mathbf{in}}.\hat{d}_{ij})(\hat{e}^{\mathbf{out}}.\hat{d}_{ij}) \vec{S}_i.\vec{S}_j \qquad \text{(A1)}$$

where $\hat{\rm d}_{\rm ij}$ are the unit vectors that connect lattice sites i and j belonging to opposite magnetic sublattices, $\rm J_{ij}$ are the corresponding exchange constants, and $\hat{\rm e}^{\mathbf{in}}$ and $\hat{\rm e}^{\mathbf{out}}$ are the incident (in) and detected (out) light polarizations, respectively.

The exchange constants involved in Eq. (1) are obtained from previous inelastic neutron scattering studies using a linear Heisenberg Hamiltonian with five nearest-neighbor Ni^{2+} spins with its exchange constants $\rm J_{ac}$, $\rm J_{bc}$, $\rm J_{ab}$, $\rm J_b$ and $\rm J_c$ [see Fig. 1(b)], and two anisotropy parameters, which proved to be sufficient to describe the observed magnon dispersions [9, 10]. Such Hamiltonian is written as:

$$\mathcal{H} = \sum_{\langle \rm i,j \rangle} \rm J_{ij} \vec{S}_i.\vec{S}_j + D_x \sum_i (S_i^x)^2 + D_y \sum_i (S_i^y)^2 \qquad \text{(A2)}$$

where D_x and D_y are anisotropy parameters.

In the case of lithium orthophosphates, only $\rm J_{ab}$ and $\rm J_{bc}$ exchange interactions, which are related to the unit vectors directions $\hat{d}_{ab} = (\pm a/\sqrt{a^2+b^2}, \pm b/\sqrt{a^2+b^2}, 0)$ and $\hat{d}_{bc} = (0, \pm b/\sqrt{b^2+c^2}, \pm c/\sqrt{b^2+c^2})$, where a, b, and c are the lattice parameters, may produce the $S = 0$ two-magnons described by the FL theory. The following symmetry proportionality relations are obeyed between the FL operators:

$$\mathcal{O}_{\rm FL}^{\mathbf{zz}} = \frac{\rm c}{\rm b} \mathcal{O}_{\rm FL}^{\mathbf{zy}} = \rm c^2 \mathcal{O}_{\rm FL}^{[\hat{\mathbf{d}}_{\mathbf{bc}}]} = \mathbf{c^2} \frac{\rm J_{bc}}{\mathbf{b^2 + c^2}} \sum_{\hat{\rm d}_{\rm bc}} \vec{S}_i.\vec{S}_j \qquad \text{(A3)}$$

$$\mathcal{O}_{\rm FL}^{\mathbf{xx}} = \frac{\rm a}{\rm b} \mathcal{O}_{\rm FL}^{\mathbf{xy}} = \rm a^2 \mathcal{O}_{\rm FL}^{[\hat{\mathbf{d}}_{\mathbf{ab}}]} = \mathbf{a^2} \frac{\rm J_{ab}}{\mathbf{a^2 + b^2}} \sum_{\hat{\rm d}_{\rm ab}} \vec{S}_i.\vec{S}_j \qquad \text{(A4)}$$

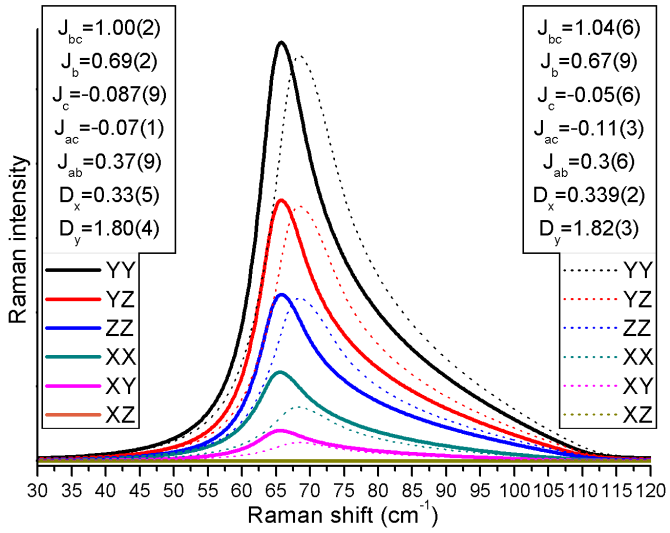

FIG. A1: Comparison between calculated two-magnon Raman spectra of $LiNiPO_4$ for different polarizations for the exchange and anisotropy parameters reported by Jensen et al. [9] and for the refined parameters obtained with the simulated annealing procedure explained in the text, in units of meV.

$$\mathcal{O}^{\mathbf{yy}}_{\mathrm{FL}} = \mathrm{b}^2(\mathcal{O}^{[\hat{\mathbf{d}}_{\mathbf{bc}}]}_{\mathrm{FL}} + \mathcal{O}^{[\hat{\mathbf{d}}_{\mathbf{ab}}]}_{\mathrm{FL}}) \tag{A5}$$

$$\mathcal{O}^{\mathbf{xz}}_{\mathrm{FL}} = 0 \tag{A6}$$

where $\mathcal{O}^{[\hat{\mathbf{d}}_{\mathbf{bc}}]}_{\mathrm{FL}}$ and $\mathcal{O}^{[\hat{\mathbf{d}}_{\mathbf{bc}}]}_{\mathrm{FL}}$ are two auxiliary operators.

The polarized two-magnon Raman signal is given by [12]:

$$\mathrm{I}^{(\mathbf{in})(\mathbf{out})}_{\mathrm{FL}}(\hbar\omega)\alpha \sum_{\mu} |\langle\mu|\mathcal{O}^{(\mathbf{in})(\mathbf{out})}_{\mathrm{FL}}|0\rangle|^2\delta(\hbar\omega - \hbar\omega_{\mu}) \tag{A7}$$

where $|0\rangle$ is the fully oriented ground spin state, $|\mu\rangle$ is the two-magnon excited state with two-magnons, and $\hbar\omega_{\mu}$ is the two-magnon excitation energy. In our calculations, magnon-magnon interactions are ignored and the δ function is replaced by a more realistic Lorentzian lineshape to capture spin-wave damping convoluted with instrumental broadening effects.

A direct consequence of the signal that comes from the polarized FL operator symmetry is that these theoretical two-magnon signals have similar shapes and positions, changing almost only in magnitude for the different polarizations, such as illustrated in Fig. A1.

In the fitting using a simulated annealing procedure shown in Fig. 4 (see also Ref. [12]), the free parameters were allowed to vary by more than one order of magnitude with respect to the initial values. Independent scale parameters were introduced for each polarization. The initial values of the exchange constants and anisotropy terms were taken from Ref. [9]. Alternative initial values were also tested in the fits, with no impact in the final converged result.

II. ACKNOWLEDGMENTS

Work at UNICAMP was conducted with financial support from FAPESP Grants 2017/10581-1 and No. 2018/20142-8, and CNPq Grants. No. 409504/2018-1 and No. 308607/2018-0, Brazil. Ames Laboratory is supported by the US Department of Energy, Office of Basic Energy Sciences, Division of Materials Sciences and Engineering under Contract No. DE-AC02-07CH11358.

[1] Santoro, R.P and Newham, R.E., Antiferromagnetism in $LiFePO_4$. Acta Cryst. **22**, 344 (1967).
[2] Santoro, R.P., Segal, D.J. and Newnham, R.E., Magnetic properties of $LiCoPO_4$ and $LiNiPO_4$. J. Phys. Chem. Solids **27**, 1192 (1966).
[3] Li, J., Tian, W., Chen, Y., Zarestky, J.L., Lynn, J.W., and Vaknin, D., Antiferromagnetism in the magnetoelectric effect single crystal $LiMnPO_4$. Phys. Rev. B **79**, 144410 (2009).
[4] A.K. Padhi, K.S. Nanjundaswamy, and J.B. Goodenough, Phospho-olivines as positive-electrode materials for rechargeable lithium batteries. Journal of the Electrochemical Society **144**, 1188 (1997).
[5] Jensen, T.B.S., Christensen, N.B., Kenzelmann, M., Ronnow, H.M., Niedermayer, C., Andersen, N. H., Lefmann, K., Schefer, J., Zimmermann, M. v., Li, J., Zarestky, J. L., and Vaknin, D., Field-induced magnetic phases and electric polarization in $LiNiPO_4$. Phys. Rev. B **79**, 092412 (2009).
[6] Abrahams, I., and Easson, K.S., Structure of lithium nickel phosphate. Acta Crystallogr., Sect. C: Cryst. Struct. Commun. **49**, 925 (1993).
[7] Yamauchi, K., and Picozzi, S., Magnetic anisotropy in Li-phosphates and origin of magnetoelectricity in $LiNiPO_4$. Phys. Rev. B **81**, 024110 (2010).
[8] Toft-Petersen, R., Fogh, E., Kihara, T., Jensen, J., Fritsch, K., Lee, J., Granroth, G.E., Stone, M.B., Vaknin, D., Nojiri, H., and Christensen, N.B., Field-induced reentrant magnetoelectric phase in $LiNiPO_4$. Phys. Rev. B **95**, 064421 (2017).
[9] Jensen, T.B.S., Christensen, N. B., Kenzelmann, M., Ronnow, H. M., Niedermayer, C., Andersen, N. H., Lefmann, K., Jiménez-Ruiz, M., Demmel, F., Li, J., Zarestky J. L., and Vaknin, D., Anomalous spin waves and the commensurate-incommensurate magnetic phase transition in $LiNiPO_4$. Phys. Rev. B **79**, 092413 (2009).
[10] Li, J., Jensen, T.B.S., Andersen, N.H., Zarestky, J.L., McCallum, R.W., Chung, J.-H., Lynn, J.W., and Vaknin, D., Tweaking the spin-wave dispersion and suppressing the incommensurate phase in $LiNiPO_4$ by iron substitution. Phys. Rev. B **79**, 174435 (2009).
[11] Toft-Petersen, R., Jensen, J., Jensen, T.B.S., Andersen, N.H., Christensen, N.B., Niedermayer, C., Kenzelmann, M., Skoulatos, M., Le, M.D., Lefmann, K., Hansen, S.R.,

Li, J., Zarestky, J.L., and Vaknin, D., High-field magnetic phase transitions and spin excitations in magnetoelectric $LiNiPO_4$. Phys. Rev. B **84**, 054408 (2011).

[12] Calderon, C.J., Gomes, P.F., García-Flores, A.F., Barberis, G.E., and Granado, E., Two-magnon Raman scattering in $LiMnPO_4$. J. Magn. Magn. Mater., **377**, 430 (2015).

[13] Fleury, P. A., and Loudon, R., Scattering of Light by One- and Two-Magnon Excitations. Phys. Rev. **166**, 514 (1968).

[14] L. Peedu, V. Kocsis, D. Szaller, J. Viirok, U. Nagel, T. Rõõm, D.G. Farkas, S. Bordács, D.L. Kamenskyi, U. Zeitler, Y. Tokunaga, Y. Taguchi, Y. Tokura, and I. Kézsmárki, Spin excitations of magnetoelectric $LiNiPO_4$ in multiple magnetic phases, Phys. Rev. B **100**, 024406 (2019).

[15] Fomin, V.I., Gnesdilov, V.P., Kurnosov, V.S., Peschanskii, A.V., Schmid, H., Rivera, J.-P., and Gentil, S., Raman scattering in $LiNiPO_4$ single crystal. Low Temp. Phys. **28**, 203 (2002).

[16] Paraguassu, W., Freire, P.T.C., Lemos, V., Lala, S. M., Montoro, L. A., and Rosolen, J.M., Phonon calculation on olivine-like $LiMPO_4$ (M = Ni, Co, Fe) and Raman scattering of the iron-containing compound. J. Raman Spectrosc. **36**, 213 (2005).

[17] Eliott, R.J., and Loudon, R., The possible observation of electronic Raman transitions in crystals. Phys. Lett. **3**, 189 (1963).

[18] Y. N. Kharchenko, N. F. Kharcheno, M. Baran, and R. Szymczak, Weak ferromagnetism and an intermediate incommensurate antiferromagnetic phase in $LiNiPO_4$, Low Temp. Phys. **29**, 579 (2003).

[19] S. Lewinska, A. Szewczyk, M.U. Gutowska, J. Wieckowski, R. Puzniak, R. Diduszko, A. Reszka, B.J. Kowalski, Yu. Kharchenko, and J. Molenda, Magnetic susceptibility and phase transitions in $LiNiPO_4$, Phys. Rev. B **99**, 214440 (2019).

[20] Devereaux, T.P. and Hackl R., Inelastic light scattering from correlated electrons. Rev. Mod. Phys. **79**, 175 (2007).

[21] Chen, C.-C., Jia, C.J., Kemper, A.F., Singh, R.R.P., and Devereaux, T.P., Theory of Two-Magnon Raman Scattering in Iron Pnictides and Chalcogenides. Phys. Rev. Lett. **106**, 067002 (2011).